ELSEVIER

NeuroImage

www.elsevier.com/locate/ynimg
NeuroImage 22 (2004) 120–133

An integrative MEG–fMRI study of the primary somatosensory cortex using cross-modal correspondence analysis

Matthias Schulz,[a,b] Wilkin Chau,[a] Simon J. Graham,[b,c] Anthony R. McIntosh,[b] Bernhard Ross,[a,b] Ryouhei Ishii,[b] and Christo Pantev[a,b,*]

[a] *Institute for Biomagnetism and Biosignalanalysis, Münster University Hospital, University of Münster, Münster, Germany*
[b] *Rotman Research Institute for Neuroscience, Baycrest Centre for Geriatric Care, University of Toronto, Toronto, Ontario, Canada*
[c] *Imaging Research, Sunnybrook and Women's College Health Sciences Centre, and Department of Medical Biophysics, University of Toronto, Toronto, Ontario, Canada*

Received 12 June 2003; revised 16 October 2003; accepted 22 October 2003

We develop a novel approach of cross-modal correspondence analysis (CMCA) to address whether brain activities observed in magnetoencephalography (MEG) and functional magnetic resonance imaging (fMRI) represent a common neuronal subpopulation, and if so, which frequency band obtained by MEG best fits the common brain areas. Fourteen adults were investigated by whole-head MEG using a single equivalent current dipole (ECD) and synthetic aperture magnetometry (SAM) approaches and by fMRI at 1.5 T using linear time-invariant modeling to generate statistical maps. The same somatosensory stimulus sequences consisting of tactile impulses to the right sided: digit 1, digit 4 and lower lip were used in both neuroimaging modalities. To evaluate the reproducibility of MEG and fMRI results, one subject was measured repeatedly.

Despite different MEG dipole locations and locations of maximum activation in SAM and fMRI, CMCA revealed a common subpopulation of the primary somatosensory cortex, which displays a clear homuncular organization. MEG activity in the frequency range between 30 and 60 Hz, followed by the ranges of 20–30 and 60–100 Hz, explained best the defined subrepresentation given by both MEG and fMRI. These findings have important implications for improving and understanding of the biophysics underlying both neuroimaging techniques, and for determining the best strategy to combine MEG and fMRI data to study the spatiotemporal nature of brain activity.

Keywords: Magnetoencephalography; Functional magnetic resonance imaging; Somatosensory cortex; Multimodal neuroimaging

Introduction

Despite the ubiquitous use of functional magnetic resonance imaging (fMRI) in neuroscience research, much remains to be determined about the relationship between fMRI signals and measures of neural activity obtained by other functional neuroimaging methods. This paper discusses these issues through a detailed examination of how fMRI and magnetoencephalography (MEG) signals are linked. The rationale for such examination is provided by brief background on the characteristics and complementary nature of fMRI and MEG signals, forming the basis for an integrative study of somatosensory cortex by means of both imaging methods.

The fMRI signal is a complex function of multiple physical parameters: blood flow, blood volume and blood oxygenation (Buxton et al., 1998; Friston et al., 2000). Most often, fMRI studies use the blood oxygen level-dependent (BOLD) signal contrast as a surrogate marker of neuronal activity (Ogawa and Lee, 1990a; Ogawa et al., 1990b,c; Ogawa et al., 1992). Compared to the fast physiological changes of neuronal cell assemblies, the BOLD fMRI signal is constrained by slow temporal dynamics. The BOLD signal reaches its maximum at 4–6 s after brief neural activation and returns to baseline within 12–14 s (Bandettini et al., 1993; Blamire et al., 1992). Furthermore, residual effects might last for up to 1 min (Fransson et al., 1999). Hence, it is not possible to characterize ongoing brain activity in real-time by this method. However, recent studies have taken advantage of the reliable timing of the evoked blood flow signal and demonstrate temporal resolution at the subsecond level (Burock et al., 1998; Menon et al., 1998; Rosen et al., 1998).

The spatial resolution of BOLD fMRI is thought to be generally better than other functional neuroimaging techniques, such as single photon emission computed tomography (SPECT), positron emission tomography (PET), electroencephalography (EEG) and MEG. However, the BOLD signal measures neuronal activity indirectly via its assumed hemodynamic correlate. The spatial resolution of the BOLD signal consequently depends on the local vascular geometry and physiology (Harrison et al., 2002). Therefore, areas with high vascular density, such as primary sensory areas, motor areas and perhaps Wernicke's and Broca's speech areas, are more likely to "light up" in fMRI (Harrison et al., 2002). A further complication is that fMRI signals reflect pooled activity of a large number of neurons (Scannell and Young, 1999).

* Corresponding author. Institute for Biomagnetism and Biosignalanalysis, Münster University Hospital, University of Münster, Kardinal-von-Galen-Ring 10, 48129 Münster, Germany. Fax: +49-251-835-6874.
E-mail address: pantev@uni-muenster.de (C. Pantev).
Available online on ScienceDirect (www.sciencedirect.com.)

1053-8119/$ - see front matter © 2004 Elsevier Inc. All rights reserved.
doi:10.1016/j.neuroimage.2003.10.049

MEG detects weak magnetic fields generated by the flow of intracellular postsynaptic currents (Hari and Forss, 1999; Hari et al., 1980; Williamson and Kaufman, 1981) of pyramidal cells, which constitute two-thirds of the neurons of the cerebral cortex (Creutzfeldt, 1995). The dynamics of these neurons can be observed precisely in both time and frequency domains. It has been estimated that a small area of about 40 mm^2 including tens of thousand synchronous active neurons can yield a net dipole moment of about 10 nAm, strong enough to be detected extracranially by MEG (Hamalainen, 1993). However, signal from neurons without an orderly orientation, such as interneurons or those in the cerebellum or white matter (Kakigi et al., 2000), may cancel out, and thus their activation is not detectable by MEG. In addition, due to detector geometry, MEG is principally sensitive to sources that are oriented tangentially to the skull, and much less sensitive to those oriented radially. Hence, MEG is constrained to cortical areas that are bounded in the walls of fissural cortex and the amplitude of the measured MEG signal decreases rapidly as the source depth increases. The results and the interpretation of MEG depend heavily on the methods used to represent neural activity in space.

The most widely used model for estimating MEG sources is the equivalent current dipole (ECD), providing a reliable estimate of activation in a focal circumscribed cortical area (Gallen et al., 1994; Pantev et al., 1991). In this case, the ECD can suitably represent the center of the neuronal activity by a point-like single source, providing, in addition to the location and orientation, the time course of the cortical source strength. The main problem of the ECD approach, however, is the nonuniqueness of the inverse solution, that is, theoretically an infinite number of source formations can explain an externally measured magnetic field distribution (Helmholtz, 1853). Thus, the use of the ECD for modeling higher cognitive functions with unknown or multiple complex source patterns is difficult and often unsatisfactory. Beyond the ECD, numerous alternative models have been developed for situations in which multiple sources can be assumed, including spatiotemporal multiple source models (MUSIC and RAP-MUSIC; Mosher and Leahy, 1998; Scherg and Ebersole, 1993; Scherg and von Cramon, 1985; Scherg et al., 1999), instantaneous minimum norm models (Fuchs et al., 1999; Hamalainen and Ilmoniemi 1994; Matsuura and Okabe, 1997; Uutela et al., 1999) and spatial, temporal and probabilistic weights minimum norm models (Phillips et al., 1997). An alternative approach is the synthetic aperture magnetometry (SAM), a novel nonlinear constrained minimum variance beamformer method, which does not provide an inverse solution and, unlike ECD, requires no a priori specification of the number of active sources. With respect to comparing or even integrating MEG and fMRI data, SAM appears to be highly appropriate. Like fMRI, it promotes a block design paradigm and it displays the three-dimensional distribution of the differences in brain activation between states of "activation" and "rest", together with the time course of cortical activation on a millisecond time scale.

Extensive literature is devoted to the investigation of the human somatosensory cortex by either fMRI or MEG. Using tactile stimulation of the hand, fMRI studies observed activity in the contralateral primary somatosensory cortex (SI); (Kurth et al., 1998; Moore et al., 2000; Polonara et al., 1999; Stippich et al., 1999), bilaterally in the secondary somatosensory cortices (SII) (Maldjian et al., 1999; Polonara et al., 1999), the parietal ventral area (PV) (Disbrow et al., 2000a; Disbrow et al., 2001), posterior parietal cortex (PPC) (Kurth et al., 2000), and other associated regions, such as cerebellum, thalamus and claustrum (Bushara et al., 2001; Davis et al., 1998). The main contribution to the BOLD activity of SI appears to come from Brodmann areas 1, 3b, and to a lesser degree from areas 2, 4 and 3a (Kurth et al., 1998, 2000; Lin et al., 1996), although these observations stem at least in part from the varied characteristics of the somatosensory stimuli applied.

Transient somatosensory-evoked-fields (SEFs) were observed by means of MEG from SI (Brodman areas 3b and 4) mainly contralaterally (20–60 ms after stimulus onset) (Forss et al., 1994; Suk et al., 1991), but also ipsilaterally to the side of stimulation (90–287 ms) (Korvenoja et al., 1995). Further bilateral generators have been reported from SII at about 100 ms (Hari et al., 1984, 1993); from PPC (70–110 ms) (Forss et al., 1994); and from mesial cortex (110–140 ms) (Forss et al., 1996). Only a limited number of MEG studies have reported activity of the thalamus and the cerebellum (Tesche, 1996; Tesche and Karhu, 1997). In addition, slow-wave and oscillatory activity have been observed: sigma rhythm from SII (Narici et al., 2001), sustained activation of SII (Forss et al., 2001), event-related desynchronization (ERD) and event-related synchronization (ERS) in the alpha-, beta- and gamma-frequency range from SI (Hirata et al., 2002), high-frequency oscillations up to 600 Hz in SI (Curio et al., 1994; Hashimoto et al., 1996; Haueisen et al., 2001) and steady-state-responses (SSR) from SI (Diesch et al., 2001; Pollok et al., 2002).

Currently, there is increasing scientific interest in addressing how well the neuronal and the hemodynamic changes correlate with brain functions. Progress in understanding this issue is possible through combined electrophysiological and fMRI measurements (Dubowitz et al., 1998; Logothetis et al., 1999, 2001; Stefanacci et al., 1998). Disbrow et al. (2000b) showed an overall concordance of 55% between fMRI and electrophysiologically defined maps. In the concordant maps, the focal points of the fMRI activations were located within the respective location obtained by using microelectrode-recording technique. However, in 45% of the cases, the center of the fMRI maps fell outside the electrophysiologically defined maps. Arthurs et al. (2000) showed linear coupling between fMRI and ERP amplitude in four out of five subjects for the early N20-P22 amplitude. Moreover, the intensity of the BOLD signal correlated linearly with the evoked potential amplitude in four of the five subjects studied. Differences in location of brain activity between MEG (ECD approach) and fMRI were reported for the early SI response (Kober et al., 2001; Stippich et al., 1998). However, in these studies, MEG and fMRI used different time intervals for the comparison: tens of milliseconds in MEG and several seconds in fMRI. Therefore, it is not clear whether the observed differences are due to the method used or to differences of the quantified activity.

Therefore, the objective of this study is to establish whether MEG and fMRI could detect a common brain subspace despite the different specificity of each measurement and the different signal-to-noise ratios inherent in each method. Furthermore, the contributions of different frequency bands of the MEG to the BOLD signal in the defined subspace should be visualized. A novel method of cross-modal correspondence analysis (CMCA) was developed to compare the MEG and fMRI signals. The CMCA was experimentally evaluated intra- and inter-individually on the brain activity evoked by somatosensory stimulation. The CMCA analysis attempts to focus on the same time window in MEG and fMRI and provides the distribution of the representation of the common subspace.

Methods

Subjects

Fourteen right-handed subjects (five female) in the ages of 24–52 years (mean of 30 years) participated in one MEG and one fMRI session. To evaluate the reproducibility of the intra-individual data, one subject was measured 10 times with MEG and 5 times with fMRI. All subjects had no history of neurological disorders. Handedness was established using the Edinburgh handedness questionnaire (Oldfield, 1971). Informed consent was obtained from each subject after the nature of the study has been explained, in accordance with the principles of the Declaration of Helsinki.

Somatosensory stimulation

A computer-controlled portable multi-channel device generated and delivered identical somatosensory stimulus sequences during MEG and fMRI measurements. Balloon diaphragms of 1 cm in diameter presented haptic stimuli independently to the palmar, distal phalanges of the right digit 1 and the right digit 4, as well as to the right side of the lower lip. The diaphragms were driven by air pressure pulses of 50 ms duration and evoked a soft sensation at the target body part. Since the stimuli applied to the digits evoked subjectively weaker sensations than those to the lip, two balloon diaphragms were used in parallel for each digit, whereas only one was used for the lower lip.

The time course of the stimulus sequence is illustrated in Fig. 1. Each body part was stimulated at a rate of 2 Hz in blocks of 15 s duration. Each block was followed by a 15-s resting period. The order of stimulated body parts was randomized between successive blocks with the restriction that the same body part was stimulated no more than two blocks in a row. A total of 450 stimuli was presented to each body part. For MEG, the entire stimulus sequence of about 23 min was recorded at once. For fMRI, the sequence was partitioned into three separate runs of 7.5 min duration to ensure that subjects remained still. An initial period of 10 s was discarded from each fMRI run to ensure that the magnetization reached equilibrium before the beginning of data collection.

MEG data collection

MEG recordings were carried out in a magnetically shielded room using a 151-channel whole-head neuromagnetometer system (Omega, CTF Inc.), equipped with axial first-order gradiometers (2 cm coil diameter and 5 cm baseline) (Vrba et al., 1998). The MEG signals were 200 Hz low-pass filtered, digitized, and sampled at the rate of 625 Hz. A head-based Cartesian coordinate system was defined for the source localization by three fiducial points, the nasion and the entrances of the left and right ear canals. Before and after each MEG recording, these points were determined by detecting the magnetic signals transmitted by three positioning coils, placed at the fiducials. The origin of the coordinate system was set at the midpoint of the medial–lateral axis (y-axis) which joined the center points of the entrance to the ear canal of the left and the right ears (positive toward the left ear). The posterior–anterior axis (x-axis) was oriented from the origin to the nasion (positive toward the nasion) and the inferior–superior axis (z-axis) was perpendicular to the x–y plane (positive toward the vertex). A sketch of the coordinate system is shown in Fig. 4.

MEG dipole analysis

Stimulus-related epochs of the recorded magnetic field data were averaged in the time domain selectively according to the stimulated body part. The DC offset was corrected with respect to a 100-ms pre-stimulus interval. Source analysis was based on a single ECD model. Dipole locations were estimated independently for seven sampling points around the first prominent peak arising at the latency of 35–55 ms in the digit response and for five

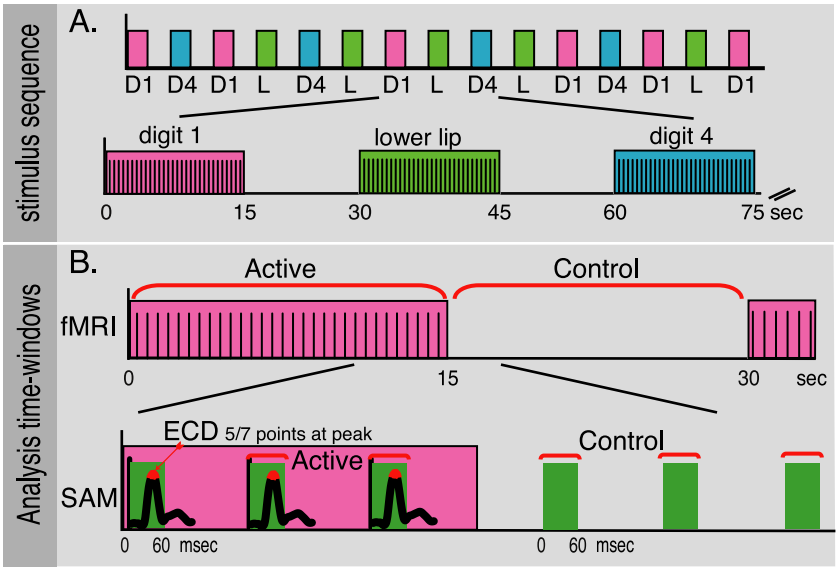

Fig. 1. (A) The pseudo-random order of stimulated thumb (digit 1, D1), digit 4 (D4) and lower lip (L) within a stimulus sequence. No body part was repeatedly stimulated more than twice in a row. In a single stimulus block, one body part was stimulated at the rate of 2 Hz during 15 s followed by a 15-s resting period. (B) Time intervals selected for the ECD, SAM and fMRI data analysis. For fMRI, a box-car design was used with a 15-s active and a 15-s control window. The interval of 60 ms duration after the onsets of each of the 30 tactile stimuli was the SAM window in the active condition. Corresponding control intervals of the same duration followed 15 s later during the stimulus-free period. For the ECD, five or seven points around the first prominent peak in the SEF waveforms were chosen.

sampling points around the peak at the latency of 20–50 ms for the lower lip response (Fig. 1). The mean source location parameters across the five or seven data points, respectively, were used for statistical evaluation. The estimated ECD coordinates of all measured subjects met the criteria of goodness of fit (R^2 value of the regression) larger than 88%, estimated locations within plausible coordinates (4.0–1.0 cm in anterior–posterior, 3.0–6.5 cm medial–lateral, and 11–5.5 cm inferior–superior direction) and were therefore accepted for further analysis.

MEG wavelet analysis

To determine the time interval and frequency range of interest for SAM, a wavelet analysis was used to characterize the averaged evoked response from SI. A wavelet filter-bank analysis in the time interval from −50 to 400 ms and the frequency range from 10 to 120 Hz was performed on the MEG time series. The MEG signals were convolved by complex Morlet-wavelet, which has a Gaussian shape in the time and frequency domain, providing optimal time–frequency resolution. The complex spectral power was calculated for each epoch and averaged across channels and epochs. The spectral amplitudes were normalized by the maximum value at each frequency, which accounted for the low-pass frequency characteristic of MEG signals.

Synthetic aperture magnetometry

SAM was used to reconstruct cortical tomographic maps, representing a statistical evaluation of signal power differences between predefined time intervals for the "active" and the "control" conditions. A basic assumption in SAM is that each possible neural source has a unique time course and any covariance with other sources will be treated as noise. To isolate the activity at any location within the brain, a spatial filter is constructed in a way that is specific to each location and that exploits the temporal correlations of the multi-channel magnetic field data. The spatial filters are based on the concept of a nonlinear constrained minimum variance beamformer (Robinson and Vrba, 1998; Widrow and Stearns, 1985). These spatial filters are optimized so that activity at the target location is emphasized and the co-varying signals from all other locations are attenuated. The signal power in a specified frequency band as estimated by the spatial filters is normalized to the estimated noise in the corresponding voxel and compared between temporal intervals related to an active and a control condition. Subsequently, a pseudo-*t* statistic, T_θ, describes the normalized power differences between the experimental conditions in each voxel:

$$T_\theta = \frac{S_A - S_C}{\sigma_A + \sigma_C}$$

where θ is the location in three-dimensional space, S_A and S_C denote the source power in the active and control window, respectively, and σ_A and σ_C denote the corresponding noise power. A voxel-wise representation of T_θ as a color-coded statistical map was then adopted for comparison with the co-registered fMRI data.

To calculate the SAM images, the head shape was first reconstructed from the anatomical MRI for each subject. In contrast to the ECD, SAM allows the spherical model to vary across the scalp surface. This makes SAM results less sensitive to the precise size and location of the sphere that is adopted. Only the channels of the left hemisphere were used or further analysis, for two reasons. First, only contralateral SI activation was expected. Secondly, using only one hemisphere avoided possible interference from correlated signals in the other hemisphere. The MEG data were band-pass filtered in three frequency bands, selected accordingly to the wavelet analysis: beta band (20–30 Hz), low gamma band (30–60 Hz) and high gamma band (60–100 Hz). Pseudo-*t* values were calculated for each voxel (reformatted to the size of 5 × 5 × 5 mm) using the time interval 0–60 ms after stimulus onset for the active window and a control window of the same duration within the stimulus-free block (c.f. Fig. 1).

To detect statistically significant activity from multiple SAM measurements within a subject and across subjects as well, a nonparametric permutation technique (Efron and Tibshiran 1993) was adapted to the SAM analysis (Chau et al., 2002). For this test, the probability distribution of T_θ was estimated by resampling the data 1024 times. For each sample, the conditions of active and resting stage were permuted within the subject and T_θ was computed for each voxel. The T_θ values were then averaged across subjects or repeated experimental sessions to obtain an average volumetric image of T_θ. To construct the distribution of the maximum T_θ from the average volumetric images for omnibus hypothesis testing, an iteration algorithm developed by Belmonte and Yurgelun-Todd (2001) was used. For each voxel, the null hypothesis of equal power in the active and resting interval was rejected at the nominal level of $P < 0.05$.

MRI data collection

Anatomical and functional MRI data were acquired with a 1.5-T MR scanner (Signa, General Electric Medical Systems, Waukesha, WI; NV/i hardware, LX 8.5 software configuration). The standard quadrature transmit/receive birdcage head coil was used. Head restraint was provided using a vacuum pillow (Vac Fix, Par Scientific, Inc.). Three fiducial markers, filled with standard MRI contrast agent (Magnevist, Berlex; 1:100 aqueous dilution by volume) were placed at the same locations used for the MEG experiments and enabled the co-registration of MRI, fMRI and MEG data. Anatomical MRI was performed using three-dimensional fast spoiled gradient echo imaging technique [128 axial slices 1.4 mm thick, field-of-view (FOV) = 22 × 18 cm, flip angle/TE/TR = 35°/6 ms/15 ms, 256 × 192 acquisition matrix] to serve as the underlay for functional maps. Functional MRI was performed using a T2*-weighted pulse sequence optimized for signal contrast arising from the BOLD effect with single shot spiral k-space readout, offline gridding, reconstruction, and correction for magnetic field inhomogeneity and Maxwell gradient terms (Glover and Lai, 1998). Imaging data were acquired as 24 coronal slices (5.0 mm thick, FOV = 20 cm, flip angle/TE/TR = 80°/40 ms/2000 ms, 64 × 64 acquisition matrix) as this orientation likely provides the best in-plane resolution for somatotopic mapping.

fMRI data analysis

Functional MRI data were analyzed using SPM99 (Wellcome Department of Cognitive Neurology, London, UK; http:/www.fil.ion.ucl.ac.uk/spm). Before statistical evaluation, preprocessing was performed using a standardized procedure (Friston et al., 1995), including the following steps: (1) *realignment*, to correct for small head motions using the first scan of the trial as reference; (2) *co-registration*, to overlay fMRI and MRI data sets accurately

in space; (3) *normalization*, to transform the imaging data for each individual into a standard stereotactic space [Montreal Neurological Institute brain template, (MNI)]; and (4) *smoothing*, to accommodate individual anatomical variability using an isotropic Gaussian filter with 8 mm full-width at half maximum (FWHM). A general linear model was used to explain signal changes at each voxel between the active and control conditions. For each individual measurement, significance between the ''active'' (stimulation) and ''control'' (rest) conditions was determined using a *t*-statistic calculated at each voxel. These results were used to identify the hotspot of the activities. To detect the random effects across measurements, the contrast images between the two conditions were pooled together. Significance was then assessed by performing a one-sample *t* test on the contrast images.

Comparison of source locations obtained from the ECD, SAM and fMRI analysis

The ECD analysis of the MEG data resulted in coordinates for SI response to stimulation of the different body parts. For both the SAM and fMRI analyses, corresponding source coordinates were obtained as the location of the largest *t* and pseudo-*t* values, respectively. All coordinates were transformed into the MNI standardized space. For this analysis, a high-resolution SAM image in the frequency range from 20 to 100 Hz was recalculated, which was sampled on 1 mm^3 voxels to reduce spatial quantization error. Mean source coordinates across the group and the repeated measurements were calculated for the three methods. The 95% confidence limits for the means were estimated from bootstrap resampling. To test whether the three methods resulted in consistent estimates of source coordinates and whether the methods distinguished between sources of the three body parts, a two-factor ANOVA [*method* (ECD, SAM, fMRI) _ *body part* (digit 1, digit 4, lip)] was performed.

MEG–fMRI correspondence

Besides comparing the MEG and fMRI source locations using the methods described above, it was determined: (a) how the task-related signals obtained by the two neuroimaging methods agreed with each other within each voxel; and (b) how the different frequency bands provided by MEG contributed to the BOLD signals. These issues were addressed using a novel multivariate method, referred as cross-modal correspondence analysis (CMCA), developed specially for this study. ''Correspondence analysis'' describes the method best, but it should be noted that the CMCA reported here is different from the established statistical method with the same name (Dettmers et al., 1996; Roux et al., 2001).

The correspondence was calculated for three frequency bands as a cross-product across all subjects between the unthresholded SAM pseudo-*t* value in each band and the unthresholded fMRI regression coefficients at each voxel (SPM contrast images) (c.f. Fig. 2). Before multiplication, the image for each subject was scaled to its absolute maximum, to eliminate biases from different scales in the two data sets. The three correspondence vectors of length equal to the number of voxels formed the rows of the correspondence matrix. A singular value decomposition (SVD)

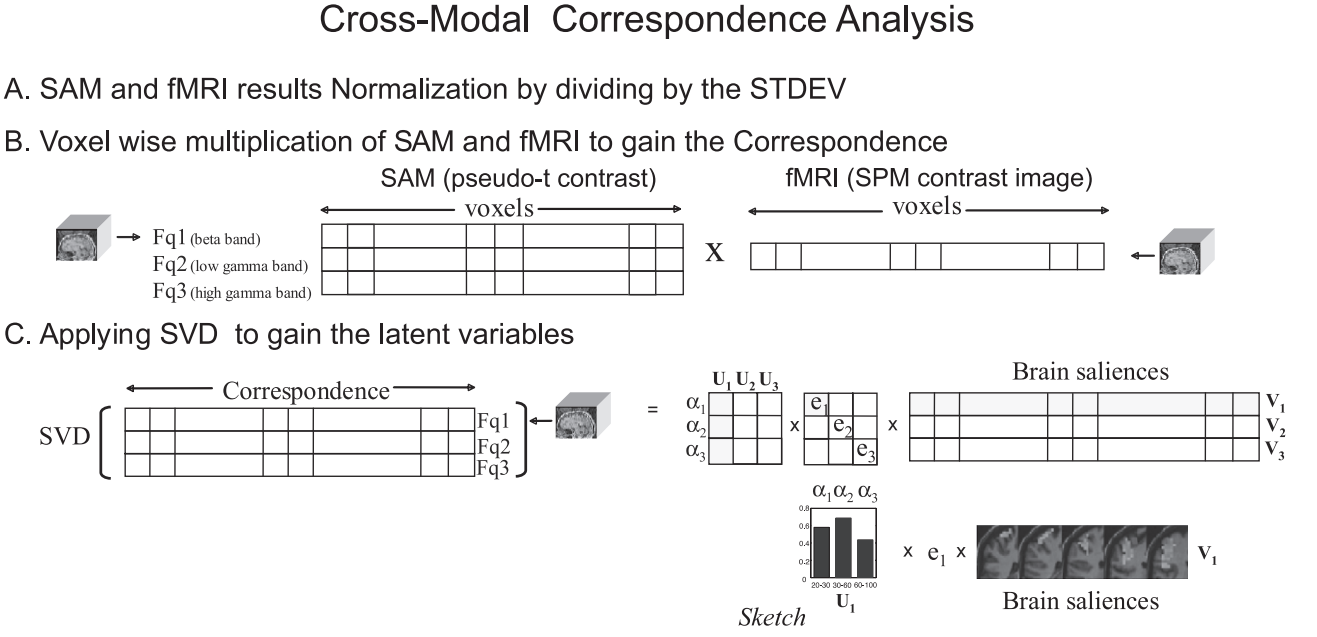

Fig. 2. Analysis steps of the cross-modal correspondence analysis. (A) The fMRI *t* values and the SAM pseudo-*t* values obtained from specified frequency bands were normalized by the corresponding standard deviations (STDEV). (B) The correspondence between fMRI and SAM in each frequency band was calculated and combined to the correspondence matrix. (C) A singular value decomposition (SVD) was performed on the correspondence matrix, resulting in pairs of latent variables (LVs). (D) Steps (A) to (C) were repeatedly performed on resampled data across the groups to test the significance of the brain salience.

decomposed the correspondence matrix into pairs of latent variables. Each pair of latent variables consists of a singular image, which is the volumetric representation of weights for each voxel, called brain salience and of weights for each frequency band. The first pair of latent variables reflects the most significant pattern of correspondence between the fMRI and MEG data. The weights reflect how each frequency band contributes to the pattern of activity observed by fMRI. The pairs of brain saliences and frequency weights are used to visualize the results of the correspondence analysis.

For statistical analysis, a bootstrap test was applied to the brain salience of each voxel. The correspondence volumes for the different frequency bands of SAM were computed for each individual measurement (n = 10 for the inter-individual and n = 5 for the intra-individual test). The data were resampled with replacement from the sets of multiple measurements. For each frequency band, the correspondence volumes were averaged across the n samples and combined into a correspondence matrix. Subsequently, a SVD was applied to this matrix, which resulted in a sample of brain salience. From resampling the data 500 times, the distribution of the brain salience of each voxel was estimated. Only those brain saliences that were reliably different from zero, based on the ratio of the estimated salience over the bootstrap-estimated standard error, were accepted for visualization and further analysis.

Results

In all MEG recordings, the ECD and SAM provided consistent cortical areas of activation. The SPM analysis of the fMRI data showed identifiable activity in SI in 12 of 14 subjects. The data from two subjects who did not show activations were excluded from the group analysis.

Wavelet analysis of evoked responses

Fig. 3 shows the global field power waveforms of the SEF and the corresponding spectrograms, obtained from maximally responding channels in responses to digit 4 and lower lip stimulation, including the data of all 10 repeated measurements. The global field power peaked around 45 ms after stimulus onset in the case of digit 4, and it was identified as the primary somatosensory response. The analogous peak occurred at 38 ms for the lower lip. In both cases, representation of the peak in the time–frequency domain indicated broad frequency contributions to the normalized power ranging from 0 up to approximately 120 Hz. In the case of lower lip stimulation, a double peak response was observed with a latency of 38 ms for the first peak. Both peaks also were narrower in the time domain than that observed for digit 4.

In both spectrograms, the pronounced spectral amplitudes after the stimulus onset show good contrast to the background MEG activity within the frequency range of 20–100 Hz. Therefore, this frequency range was selected for SAM analysis and divided into three frequency bands (beta: 20–30 Hz, low gamma: 30–60 Hz, and high gamma: 60–100 Hz). The white rectangles in Fig. 3 mark the time interval 0–60 ms and the frequency range 20–100 Hz, which were selected for SAM analysis of the SEF.

SI representation of SAM, ECD and fMRI for the single subject and the group

The ANOVA revealed significant effects of both factors *body parts* [$F(2,24) = 15.33$, $P < 0.0001$] and *methods* [$F(2,24) = 22.39$, $P < 0.0001$]. This means that all three methods separated the sources corresponding to the three body parts. However, the localization estimates were different for the different methods. The obtained source coordinates of digit 1, digit 4 and lower lip

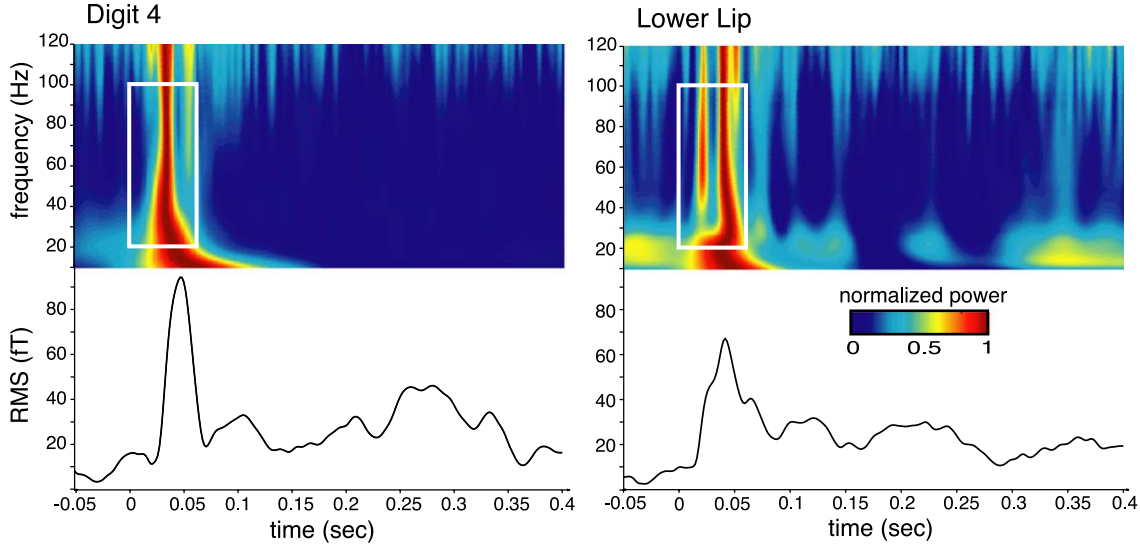

Fig. 3. Individual waveforms of the global field power (top) and time–frequency representation (bottom) of the averaged evoked response obtained from selected channels around the maximum of the magnetic field distribution averaged across 10 repetitive measures for digit 4 (left) and lower lip (right) The time scale, which is referenced to the stimulus onset, is common to the waveforms and time–frequency representations. The power, which was normalized for each frequency to the maximum within the displayed time interval, is coded on a color scale as indicated. The white rectangle marks the time–frequency interval selected for subsequent SAM analysis of the SI response.

in SI as determined by the ECD, the coordinates of the maxima of pseudo-*t* values obtained with SAM and the maxima of *t* values from the fMRI measurements are depicted for the group in Fig. 4A. The analogous results for repeated measurements of a single subject are shown in Fig. 4B. In these figures, the 95% confidence volumes, which do not overlap at least in one projection with the location of a neighbouring body part, show a clear separation of all body parts with all three methods. The labels D1 (digit 1), D4 (digit 4) and LL (lower lip), which are placed at the mean coordinates obtained with all the different methods, demonstrate the somatotopic order D4–D1–LL for the group and the repeated measurement of an individual. For the group, the somatotopic representation was most pronounced in inferior–superior direction with an extension of more than 2 cm, and extensions of about 1 cm in the anterior–posterior and less in the lateral–medial directions, respectively. For the individual, the analogous measurements were slightly larger. A projection of the source locations obtained in the group onto a three-dimensional representation of the brain surface is shown in Fig. 4C.

For a quantitative analysis of the localization differences between the methods for the different body parts, the 95% confidence limits as obtained by pairwise *t* tests using Tukey's method are summarized in Fig. 4D. The figure identifies significant localization differences if the confidence interval does not include the vertical zero line. For the group and the repeatedly measured individual, the SAM results were consistently about 5 mm more superior to the ECD locations, whereas the fMRI results were consistently 5–10 mm more inferior to the sources obtained with SAM and ECD. A similar order was found in medial–lateral direction with most medial coordinates for the SAM results, the ECD locations about 5 mm more lateral, and the fMRI location 7–9 mm more lateral than the SAM results. Both the group and repeated measurement data resulted in about 4 mm more posterior source locations for SAM compared to the ECD results. The fMRI locations obtained from the repeated individual measurements were about 7 mm more anterior than the SAM and 3 mm more anterior than the ECD results, respectively. In the group, the fMRI locations were not significantly different from those of SAM in the anterior–posterior direction, but 5 mm more posterior than the ECD locations.

The localization differences between the body parts shown on the right of Fig. 4D demonstrate the consistency between group and repeated measurements in the anterior–posterior and medial–lateral directions. In the inferior–superior direction, the separation between digit 4 and digit 1 is larger in the repeatedly measured individual than in the group. Similarly, the distance between lower

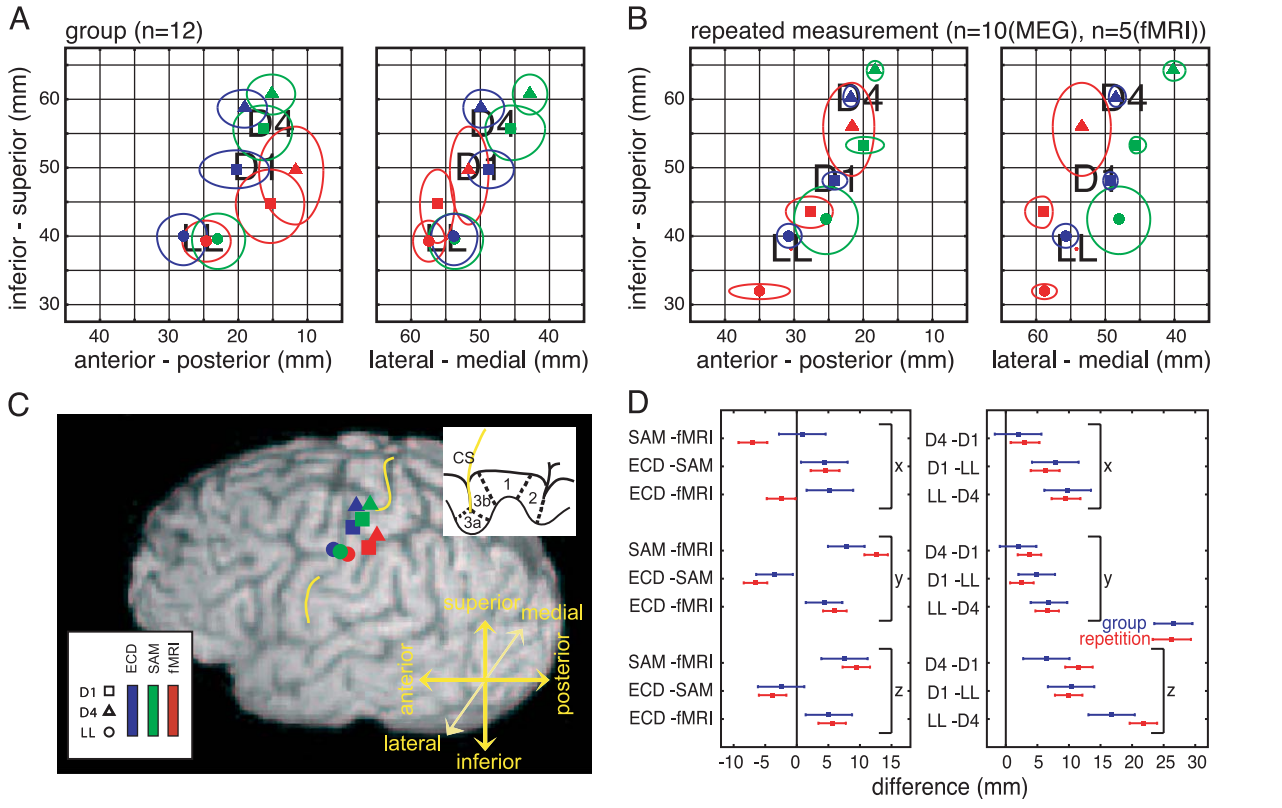

Fig. 4. (A) Inter-individual comparisons of source localizations estimated by ECD (blue), SAM (green) and fMRI (red) for the SI representations of digit 4 (triangle), digit 1 (square) and lower lip (circle). The symbols represent the mean source coordinates in the x–z plane (left) and the y–z plane (right) in combination with the 95% confidence limits of the mean shown as ellipsoids. (B) Intra-individual comparison of the results of source localization. (C) Superimposition of the group results onto the three-dimensional reconstruction of an individual brain surface. The sketch in the upper right corner outlines the Brodmann boundaries dividing the SI. (D) Results of multiple comparisons between source coordinates obtained with the different methods (left) and for the different body parts (right). The error bars denote the corrected 95% confidence intervals for the differences. Confidence intervals that do not cross the zero line indicate a significant difference.

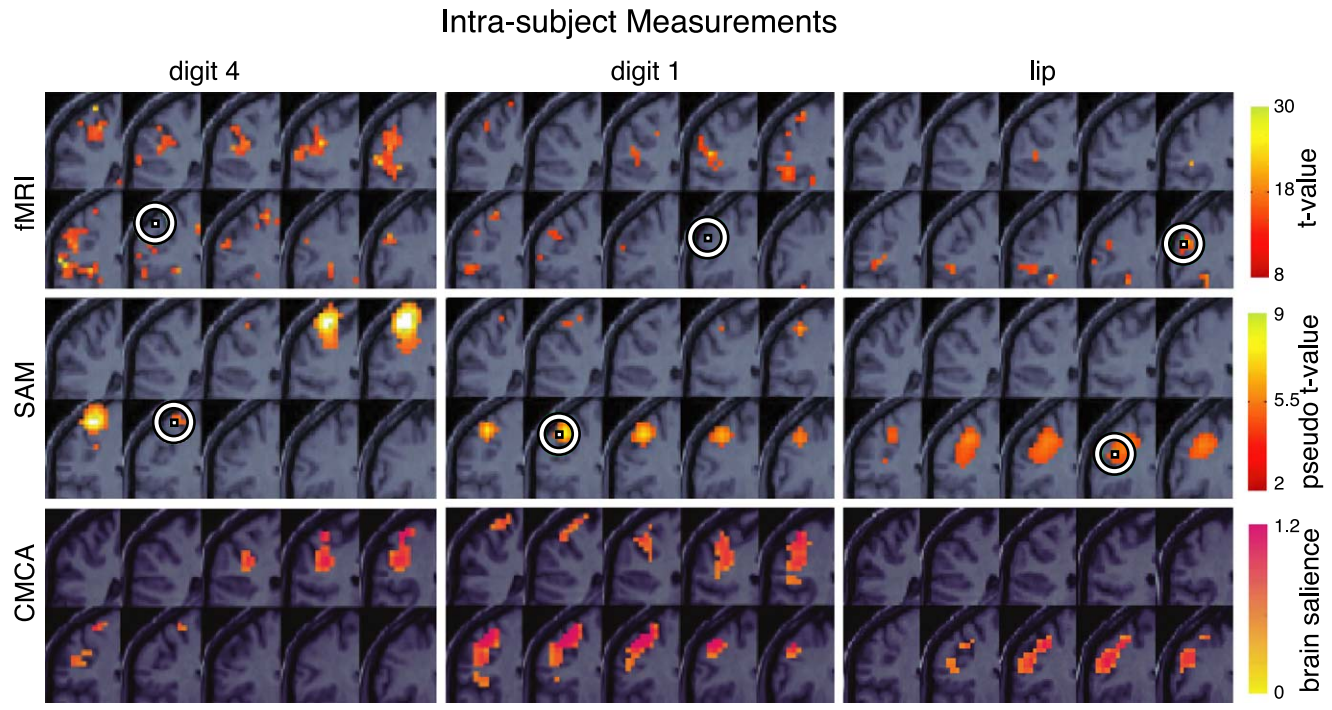

Fig. 5. Pseudo-*t* values of SAM and *t* values of fMRI analysis obtained from repeated measurements (upper and middle rows, respectively). The results corresponding to digit 1, digit 4 and lower lip stimulation are superimposed on coronal slices of the individual brain. The slices are arranged in anterior to posterior order. Only those voxels are shown that reached the (uncorrected) significance level of $P < 0.01$ fMRI, and $P < 0.05$ SAM on the basis of a permutation test. The white dots within white circles mark the mean location of the individual maxima of fMRI and SAM results (hotspots). Results of CMCA brain saliences applied to the repeated individual measurements are shown in the bottom row ($P < 0.01$, uncorrected on the basis of bootstrap resampling).

lip and digit 4 representation extends over 22 mm for the individual and 17 mm for the group in inferior–superior direction. The lip and digit 1 representation are separated by 10 mm in this direction. In the anterior–posterior direction, the somatotopic representation of the three body parts extends over 10 mm and in lateral–medial direction over 6 mm.

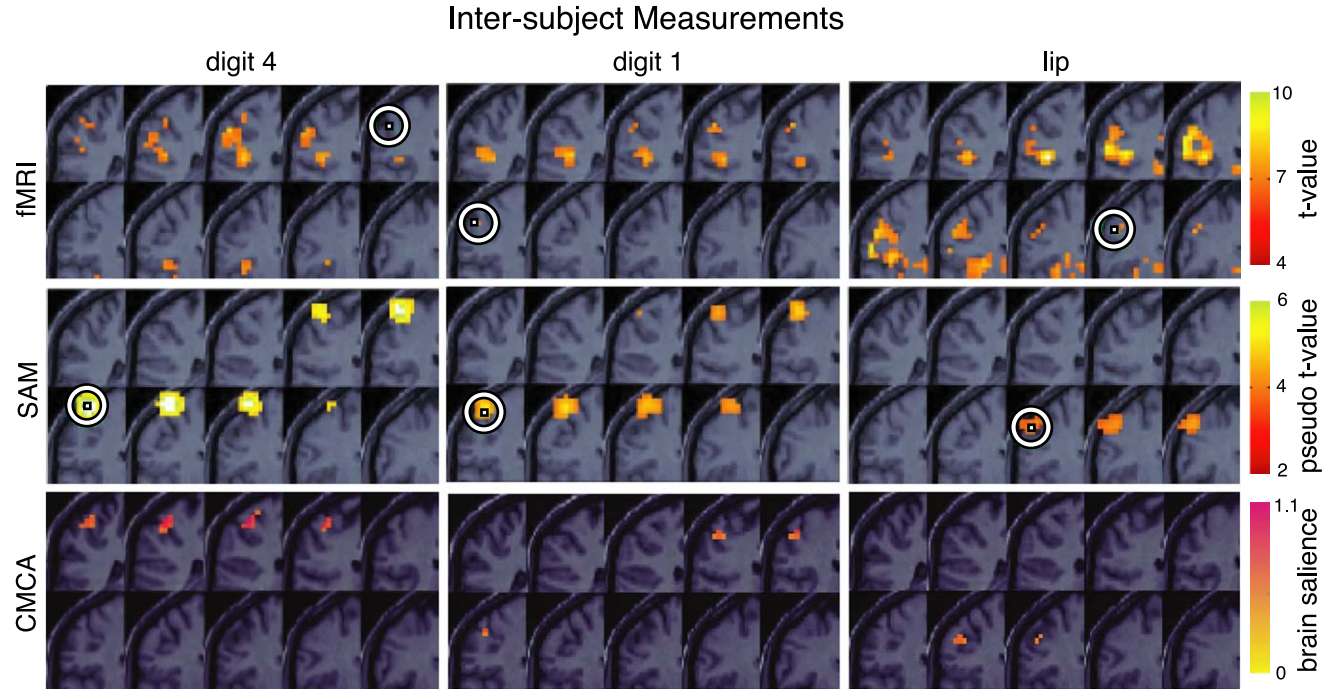

Fig. 6. Pseudo-*t* values of SAM, *t* values of fMRI analysis and CMCA results obtained from the group of 14 subjects, arranged as in Fig. 5.

SAM permutation and fMRI analysis

Figs. 5 and 6 compare the SAM permutation and fMRI results for the single subject and the group, respectively. These figures show activation maps superimposed on cropped coronal anatomical images, and provide a visual description of the location and extent of activation with respect to SI for both imaging methods. Thus, these figures encapsulate features of the brain activity not indicated by the analysis of cortical loci shown in Fig. 4. In both Figs. 5 and 6, SAM and fMRI generally identify activity in the contralateral SI. However, probably due to the selection of the time interval and the contralateral MEG channels, SAM detected only SI while fMRI depicted also the contralateral (and ipsilateral—not shown) secondary somatosensory cortex (SII). Although the regions of activity corresponding to the digit representations were not separable in both studies using SAM or fMRI, the lower lip representation was inferior compared to the digits and in line with the somatotopic cortical organization. The group fMRI had fewer active areas, which can be expected since only the common activity across subjects was detected.

Single subject analysis

In the study of the single subject, the digit 4 stimulation evoked the largest and strongest activity of all body parts (Fig. 5). The peak activity was located in the central sulcus, whereas scattered activity included the precentral gyrus, white matter and postcentral gyrus (Brodmann area, BA 1). The activity of digit 1 included the pre- and postcentral gyrus and was slightly overlapping that of digit 4. The lower lip activity was well localized, being more anterior and inferior in comparison to that of the digits. Overall, this spatial relationship agreed well with the established somatosensory homunculus.

Group analysis

Similar features were observed for the group analysis (Fig. 6). Digit 1, digit 4 and lower lip stimulation activated SI. The thumb representation was well localized and inferior to the one of digit 4. However, both representations overlapped. In contrast to the digits, the lower lip was bilaterally represented in SI with activity located more inferior and anterior.

The strongest fMRI activity of the digits was found in the contralateral SII, even stronger than the SI response. Additionally, digit 4 stimulation activated the ipsilateral cerebellum (tonsil) and bilateral insula (BA13). The lower lip activation was in general widespread, comprising SI and SII; and additionally, the cingulate gyrus, contralateral cerebellum, insula, thalamus and ipsilateral midbrain.

The SAM permutation analysis showed well-circumscribed activity in the postcentral gyrus (SI). The lip representation was inferior and anterior compared to the digits, in line with the known somatotopy.

MEG–fMRI correspondence

The CMCA in Figs. 5 and 6 illustrates the spatial concordance of the SAM and fMRI activations for the measured SAM frequency bands: 20–30, 30–60 and 60–100 Hz. The SAM frequency weights contributing to the brain salience are shown in Fig. 7. In both, the group and the repeatedly measured individual, the correspondence

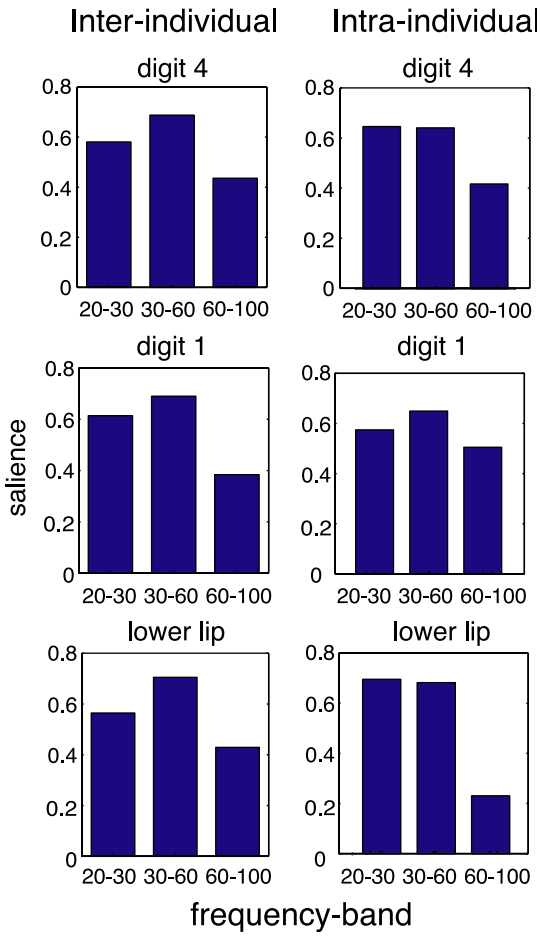

Fig. 7. Bar plots show the weights with which a distinct frequency band (20–30 Hz, 30–60 Hz, 60–100 Hz) contribute to the SAM–fMRI correspondence for the repeated measurements (right) and for the group of 14 subjects (left).

analysis revealed a common neuronal population of SI for all stimulated body parts, with a clear somatotopic organization. In some cases, the brain salience agreed with the overlap of MEG and fMRI. Overall, the CMCA locations tended to be in between the peak SAM- and fMRI-activity; mainly more posterior, more inferior and more medial as compared to the SAM activity. Additionally, the CMCA yielded new areas not seen in either imaging technique, especially posterior parietal cortex activity for digit 4 and digit 1 in the repetition study. There is an overall trend that, the low gamma-band SAM results showed the highest correspondence with the fMRI, followed by the beta- and high gamma-band.

In the group study, the CMCA marked a clear focal high brain salience in SI that is in accordance with the somatotopic organization, especially in the superior–inferior plane and in the anterior–posterior plane. No additional high brain saliences were evident. The SII activity shown in fMRI was filtered out in the correspondence analysis.

In the single-subject repetition study, the CMCA detected mainly SI and SII, and the posterior parietal cortex. The highest correspondence was found in SI where all body parts showed a somatotopic organization. The CMCA also highlighted the secondary somatosensory cortex for all stimulated body parts. Finally, a high brain salience was found in the posterior parietal cortex

following digit 1 stimulation, which was not detected with either MEG or fMRI alone.

Discussion

In this study, all three neuroimaging methods (ECD, SAM and fMRI) were able to mark the homuncular organization of the contralateral SI. In the inferior–superior direction, the distance between lower lip and digit 4 representation extends over 22 mm for the individual and 17 mm for the group. The lip and digit 1 representation are separated by 10 mm in this direction. In the anterior–posterior direction, the somatotopic representation of the three body parts extends over 10 mm and in lateral–medial direction over 6 mm. Thus, the results of this study are in line with previous findings despite differences in the imaging techniques. Both fMRI and MEG data exhibit a 12- to 18-mm tangential length to the finger region (Kurth et al., 2000; Maldjian et al., 1999). Similarly, Nakamura et al. used the ECD to detect mean linear distances between lip and digit 1 of 1.46 ± 0.70 cm and between digit 4 and digit 1 of 1.22 ± 0.23 cm (Nakamura et al., 1998).

Despite the relatively good agreement between MEG and fMRI localizations as presented in this study, significant differences between the ECD, SAM and fMRI results were found in the anterior–posterior, superior–inferior and medial–lateral directions. The following sections briefly discuss the possible reasons for the observed spatial differences and how the SAM–fMRI results are tied together through the means of CMCA.

SAM and ECD

The inconsistency between SAM and ECD likely arises due to a combination of intrinsic differences between the two techniques. ECD identifies the dipole locations based on the rhythmic neuronal changes in the active condition, whereas SAM detects the brain activities based on the source power difference between the active and control conditions. ECD uses a single local sphere for dipole fitting and therefore is very sensitive to the sphere location, whereas SAM can use different local spheres to estimate the source powers for the different locations. Lastly, ECD uses a single dipole to represent the centre of gravity of all sources such that dipole estimation is affected by distributed or distant sites of activity, whereas correlated sources are suppressed by the spatial filters in SAM. Given these differences, discrepancy between SAM and ECD is expected and the SAM results are thought to be more reflective for the spatial location of the neuronal activity. Particularly, SAM is more sensitivity to multiple sources rather than assuming a single ECD. Interestingly, there is not a clear-cut observation that SAM results and fMRI results agree better than ECD and fMRI.

MEG and fMRI

Parts of somatosensory cortex were emphasized differently between MEG and fMRI. While MEG results emphasize the SI response, in fMRI, the strongest activity was detected from SII. On reflection, this is not surprising. The SI response at 45 ms is a brief event, whereas neural activity continues to evolve over several hundred milliseconds, involving SII and more posterior regions. Therefore, it is likely that the responses associated with these regions are weighted more heavily by fMRI over the 15-s active condition. Another possibility is that fMRI "box-car" study designs may be affected by synchronization and desynchronization of neurons responding to the end or beginning of a stimulus sequence. Logothetis et al. (2001) reported that local field potentials (LFPs), which reflect superposition of synchronized dendritic currents averaged over a larger volume of tissue, are significantly better correlated with fMRI signal than multi-unit activity (MUA), which is believed to reflect spiking activity of neurons near the electrode tip.

The different SI location estimates of ECD and fMRI reported in this study are in line with Kober et al. (2001), Stippich et al., 1998 and Korvenoja et al. (1999) who found mean linear distances between ECD source locations and the centroid of the fMRI activation of 15 mm, 13.5 mm and 15 mm, respectively. The fMRI activations of BA3b were significantly more lateral and inferior compared to SAM and ECD, as found by Kober et al. (2001), and also more posterior, in agreement with Disbrow et al. (2000a). In fact, the BOLD signals for the SI areas are mainly localized posteriorly (Burton and Sinclair, 2000; Kurth et al., 1998; Moore et al., 2000; Pardo et al., 1997), close to major vasculature running in inferior–superior direction (Disbrow et al., 2000b). Furthermore, since both ECD and SAM results of this study were based on signals corresponding to a short time interval, activities in BA1 and BA2 might not have been detected by MEG as they occur about 90 ms after the stimulus onset (Allison et al., 1989; Goldring et al., 1970). However, both activities should contribute to the BOLD signal. It is not surprising that fMRI and MEG would identify different SI areas, since one is based on the synchronized neuronal activity and the other on the blood-flow-dependent changes.

MEG–fMRI correspondence

This study introduced a new procedure to analyze MEG and fMRI data to gain both scientific and statistical power by pooling data from the two methods. Intra-operative cortical mapping has shown that MEG (Gallen et al., 1995; Makela et al., 2001; Roberts et al., 1995a,b) and fMRI (Jack et al., 1994; Mueller et al., 1996; Puce et al., 1995; Yetkin et al., 1997; Yousry et al., 1995) can correctly detect neuronal sources. Similar results have been obtained by comparison with transcranial magnetic stimulation (Krings et al., 1997; Morioka et al., 1995; Roberts and Rowley, 1997). Both fMRI and MEG have individual advantages and disadvantages in locating neuronal activity, which might affect the signal-to-noise ratio differently in each method. The joint use of fMRI and MEG has been proposed by several authors (Beisteiner et al., 1997; Inoue et al., 1999; Roberts and Rowley, 1997), since each method has its own limitations (Kober et al., 2001) and emphasizes different aspects of the neuronal population. We combined both MEG and fMRI to provide a robust localization estimate and in gross a 'more realistic representation' or at least a complementary approach of the underlying neuronal representation afforded by both modalities. To proceed in this direction, we addressed here the questions (1) whether the activity observed from MEG and fMRI represents a common neuronal population, and if so (2) which frequency band obtained by MEG best fits to this neuronal subpopulation.

Despite the different SI representations measured by MEG and fMRI, CMCA depicted a common neuronal subpopulation in all

three cases. In the group measurements, CMCA showed a high correspondence between SAM and fMRI in SI. The investigated body parts followed the homuncular organization, especially in the superior–inferior plane and in the anterior–posterior plane. In the repeated measurements of an individual, CMCA depicted SII in addition to SI, and also for the digits the posterior parietal cortex. In addition, early activations of the postcentral sulcus and posterior operculum, as shown in the CMCA of the repeated measurement, agree with the observations of Korvenoja et al. (1999).

The CMCA images do not display activity in formal sense, but rather brain regions in which MEG and fMRI activation maps best match. By using unthresholded images, this approach is able to detect areas of maximal overlap between imaging modalities, which may not pass the statistical threshold in each single modality. The addition of the bootstrap assessment of CMCA results ensures that the overlap is also statistically reliable. Therefore, it was expected that CMCA displays areas not seen in either single modal analysis; hence, our study could show that (1) MEG and fMRI in case of SI correspond better than reported in previous studies, and (2) CMCA was able to detect for the repetition study activations in SII and PPC seen only to some extent in MEG or fMRI.

In line with the wavelet analysis, good correspondences were found for all selected frequency bands. The best correspondence was found for the 30- to 60-Hz frequency band followed by the 20- to 30- and 60- to 100-Hz frequency bands. However, the differences were marginal and all frequencies explained the distributed activations of fMRI almost equally well. Hence, in general, a distribution of neuronal oscillatory power, comprising all measured frequency bands, contributes to the BOLD signal following tactile stimulation.

Final remarks

The main purpose of the present study was to investigate the relationship between MEG and fMRI signals. We therefore introduced the new method of CMCA to spatially correlate specified time intervals of MEG with the BOLD fMRI signal. Pooling data from the two different modalities increased the scientific understanding and the statistical power by locating common neuronal subpopulations, which can be used for seeded dipole estimates to refine and increase the spatial and temporal selectivity power of MEG.

The primary somatosensory cortex was chosen as an example for the present study. The observations that: (1) MEG and fMRI are found to be sensitive to common neuronal subpopulations and (2) there is a broad-band frequency contribution of neuronal activity to fMRI signals, represent important additional insight into the biophysical relationship between the two imaging modalities. Furthermore, they have positive implications for development of further methods to combine MEG and fMRI to probe brain function.

Acknowledgments

We thank A. Wollbrink for technical assistance. This work was supported by the Canadian Institutes for Health Research, the Canadian Foundation for Innovation and Ontario Innovation Trust, and General Electric Medical Systems Canada.

Appendix A

SAM is based on the principle of the minimum variance beamforming technique commonly used in sonar and radar for signal detection. As an adaptive beamformer, SAM constructs a spatial filter for each location in the head, which allows passing the signals originating from the specified location while attenuating all other signals. The spatial filter for location and moment vector θ is a linear projection operator defined by a set of coefficients (⊠), with one coefficient for each sensor. Given an array of m sensor measurements, $\mathbf{M}$, the filter output at θ is represented as:

$$S_{\grave{e}} = \mathbf{W}_{\grave{e}}^{\mathrm{T}}\mathbf{M}. \tag{1}$$

To suppress signals from the unwanted location, the coefficients $\mathbf{W}_{\grave{e}}$ is chosen such that the output power is minimum while ensuring a unit response for the source at θ. Mathematically, the coefficients are determined by minimizing the source power,

$$S_{\theta}^{2} = [\mathbf{W}_{\theta}^{\mathrm{T}}\mathbf{M}] = \mathbf{W}_{\theta}^{\mathrm{T}}\mathbf{C}\mathbf{W}_{\theta}, \tag{2}$$

subject to the constraint of $\mathbf{W}_{\grave{e}}^{\mathrm{T}}\mathbf{B}_{\grave{e}} = 1$, where $\mathbf{C}$ is the covariance matrix between the sensor signals, and $\mathbf{B}_{\grave{e}}$ is the forward solution, which determines the magnetic field at the sensor locations, associated with a dipole with parameters θ. The coefficient solution is:

$$\mathbf{W}_{\theta} = \frac{[\mathbf{C} + \mu\acute{\mathbf{O}}]^{-1}\mathbf{B}_{\theta}}{\mathbf{B}_{\theta}^{\mathrm{T}}[\mathbf{C} + \mu\acute{\mathbf{O}}]^{-1}\mathbf{B}_{\theta}}, \tag{3}$$

where $\mathbf{\Sigma}$ is a diagonal matrix representing the estimated sensor noise power, and μ is the Backus-Gilbert regularization parameter adjusting the trade-off between the filter's spatial resolution and sensitivity to the uncorrelated noise. With $\mu = 0$, the obtained coefficients are the minimum variance solution which has maximum spatial selectivity; whereas, minimum-norm solution (for a single source) is obtained when μ is very large (Robinson and Vrba, 1998). Note that since the filter coefficients are chosen to attenuate the source powers from other locations, the filter would also suppress the part of signals at θ that is correlated with other sources. However, the performance of the beamformer is robust to moderate levels of correlation between sources (Van Veen et al., 1997).

After the coefficients have been determined, the power of the filtered signal is then computed using Eq. (2). Three-dimensional volume of the distribution of source powers is obtained by applying the above procedure at each location inside the head. To determine the task-related source power, the common-mode power, obtained from the period of a control state, is subtracted from the estimated source power during an active state.

The sensitivity of the MEG signals varies as a function of source location. The signal-to-noise ratio of the source estimate declines as the distance between the source and sensors increases. The noise may obscure the neural activities from the deep sources. To better estimate the source distribution, the relative strength of the source power and noise is used to generate the brain volume, which is referred to as pseudo-t value,

$$T_{\grave{e}} = \frac{S_{\grave{e}}^{\mathrm{A}} - S_{\grave{e}}^{\mathrm{C}}}{\acute{o}_{\grave{e}}^{\mathrm{A}} + \acute{o}_{\grave{e}}^{\mathrm{C}}}, \tag{4}$$

where S_θ^A and S_θ^C are the estimated power of the source for the active and control task, respectively, σ_θ^A and σ_θ^C are the estimated powers of the noise. The pseudo-*t* value can serve as the task-related neural activity index.

References

Allison, T., McCarthy, G., Wood, C.C., Williamson, P.D., Spencer, D.D., 1989. Human cortical potentials evoked by stimulation of the median nerve. II. Cytoarchitectonic areas generating long-latency activity. J. Neurophysiol. 62, 711–722.

Arthurs, O.J., Williams, E.J., Carpenter, T.A., Pickard, J.D., Boniface, S.J., 2000. Linear coupling between functional magnetic resonance imaging and evoked potential amplitude in human somatosensory cortex. Neuroscience 101, 803–806.

Bandettini, P.A., Jesmanowicz, A., Wong, E.C., Hyde, J.S., 1993. Processing strategies for time-course data sets in functional MRI of the human brain. Magn. Reson. Med. 30, 161–173.

Beisteiner, R., Erdler, M., Teichtmeister, C., Diemling, M., Moser, E., Edward, V., Deecke, L., 1997. Magnetoencephalography may help to improve functional MRI brain mapping. Eur. J. Neurosci. 9, 1072–1077.

Belmonte, M., Yurgelun-Todd, D., 2001. Permutation testing made practical for functional magnetic resonance image analysis. IEEE Trans. Med. Imag. 20, 243–248.

Blamire, A.M., Ogawa, S., Ugurbil, K., Rothman, D., McCarthy, G., Ellermann, J.M., Hyder, F., Rattner, Z., Shulman, R.G., 1992. Dynamic mapping of the human visual cortex by high-speed magnetic resonance imaging. Proc. Natl. Acad. Sci. U. S. A. 89, 11069–11073.

Burock, M.A., Buckner, R.L., Woldorff, M.G., Rosen, B.R., Dale, A.M., 1998. Randomized event-related experimental designs allow for extremely rapid presentation rates using functional MRI. NeuroReport 9, 3735–3739.

Burton, H., Sinclair, R.J., 2000. Attending to and remembering tactile stimuli: a review of brain imaging data and single-neuron responses. J. Clin. Neurophysiol. 17, 575–591.

Bushara, K.O., Wheat, J.M., Khan, A., Mock, B.J., Turski, P.A., Sorenson, J., Brooks, B.R., 2001. Multiple tactile maps in the human cerebellum. NeuroReport 12, 2483–2486.

Buxton, R.B., Wong, E.C., Frank, L.R., 1998. Dynamics of blood flow and oxygenation changes during brain activation: the balloon model. Magn. Reson. Med. 39, 855–864.

Chau, W., Ishii, R., Ross, B., McIntosh, A.R., Pantev, C., 2002. Group Analysis for the Synthetic Aperture Magnetometry (SAM) Data. Biomag.

Creutzfeldt, O.D., 1995. Cortex Cerebri. Oxford Univ. Press, Oxford.

Curio, G., Mackert, B.M., Burghoff, M., Koetitz, R., Abraham-Fuchs, K., Harer, W., 1994. Localization of evoked neuromagnetic 600 Hz activity in the cerebral somatosensory system. Electroencephalogr. Clin. Neurophysiol. 91, 483–487.

Davis, K.D., Kwan, C.L., Crawley, A.P., Mikulis, D.J., 1998. Functional MRI study of thalamic and cortical activations evoked by cutaneous heat, cold, and tactile stimuli. J. Neurophysiol. 80, 1533–1546.

Dettmers, C., Connelly, A., Stephan, K.M., Turner, R., Friston, K.J., Frackowiak, R.S., Gadian, D.G., 1996. Quantitative comparison of functional magnetic resonance imaging with positron emission tomography using a force-related paradigm. NeuroImage 4, 201–209.

Diesch, E., Preissl, H., Haerle, M., Schaller, H.E., Birbaumer, N., 2001. Multiple frequency steady-state evoked magnetic field mapping of digit representation in primary somatosensory cortex. Somatosens. Motor Res. 18, 10–18.

Disbrow, E., Roberts, T., Krubitzer, L., 2000a. Somatotopic organization of cortical fields in the lateral sulcus of *Homo sapiens*: evidence for SII and PV. J. Comp. Neurol. 418, 1–21.

Disbrow, E.A., Slutsky, D.A., Roberts, T.P., Krubitzer, L.A., 2000b. Functional MRI at 1.5 tesla: a comparison of the blood oxygenation level-dependent signal and electrophysiology. Proc. Natl. Acad. Sci. U. S. A. 97, 9718–9723.

Disbrow, E., Roberts, T., Poeppel, D., Krubitzer, L., 2001. Evidence for interhemispheric processing of inputs from the hands in human S2 and PV. J. Neurophysiol. 85, 2236–2244.

Dubowitz, D.J., Chen, D.Y., Atkinson, D.J., Grieve, K.L., Gillikin, B., Bradley Jr., W.G., Andersen, R.A., 1998. Functional magnetic resonance imaging in macaque cortex. NeuroReport 9, 2213–2218.

Efron, B., Tibshiran, R., 1993. An Introduction to the Bootstrap. Chapman and Hall, London.

Forss, N., Hari, R., Salmelin, R., Ahonen, A., Hamalainen, M., Kajola, M., Knuutila, J., Simola, J., 1994. Activation of the human posterior parietal cortex by median nerve stimulation. Exp. Brain Res. 99, 309–315.

Forss, N., Merlet, I., Vanni, S., Hamalainen, M., Mauguiere, F., Hari, R., 1996. Activation of human mesial cortex during somatosensory target detection task. Brain Res. 734, 229–235.

Forss, N., Narici, L., Hari, R., 2001. Sustained activation of the human SII cortices by stimulus trains. NeuroImage 13, 497–501.

Fransson, P., Kruger, G., Merboldt, K.D., Frahm, J., 1999. Temporal and spatial MRI responses to subsecond visual activation. Magn. Reson. Imag. 17, 1–7.

Friston, K.J., Holmes, A.P., Worsley, K.J., Poline, J.B., Frith, C.D., Frackowiak, R.S., 1995. Statistical parametric maps in functional imaging: a general linear approach. Hum. Brain Mapp. 2, 189–210.

Friston, K.J., Mechelli, A., Turner, R., Price, C.J., 2000. Nonlinear responses in fMRI: the Balloon model, Volterra kernels, and other hemodynamics. NeuroImage 12, 466–477.

Fuchs, M., Wagner, M., Kohler, T., Wischmann, H.A., 1999. Linear and nonlinear current density reconstructions. J. Clin. Neurophysiol. 16, 267–295.

Gallen, C.C., Schwartz, B., Rieke, K., Pantev, C., Sobel, D., Hirschkoff, E., Bloom, F.E., 1994. Intrasubject reliability and validity of somatosensory source localization using a large array biomagnetometer. Electroencephalogr. Clin. Neurophysiol. 90, 145–156.

Gallen, C.C., Schwartz, B.J., Bucholz, R.D., Malik, G., Barkley, G.L., Smith, J., Tung, H., Copeland, B., Bruno, L., Assam, S., et al., 1995. Presurgical localization of functional cortex using magnetic source imaging. J. Neurosurg. 82, 988–994.

Glover, G.H., Lai, S., 1998. Self-navigated spiral fMRI: interleaved versus single-shot. Magn. Reson. Med. 39, 361–368.

Goldring, S., Aras, E., Weber, P.C., 1970. Comparative study of sensory input to motor cortex in animals and man. Electroencephalogr. Clin. Neurophysiol. 29, 537–550.

Hamalainen, H., 1993. Magnetoencephalography: theory, instrumentation, and applications to noninvasive studies of the working human brain. Rev. Mod. Phys. 65, 413–497.

Hamalainen, M.S., Ilmoniemi, R.J., 1994. Interpreting magnetic fields of the brain: minimum norm estimates. Med. Biol. Eng. Comput. 32, 35–42.

Hari, R., Forss, N., 1999. Magnetoencephalography in the study of human somatosensory cortical processing. Philos. Trans. - R. Soc. Lond., B Biol. Sci. 354, 1145–1154.

Hari, R., Aittoniemi, K., Jarvinen, M.L., Katila, T., Varpula, T., 1980. Auditory evoked transient and sustained magnetic fields of the human brain. Localization of neural generators. Exp. Brain Res. 40, 237–240.

Hari, R., Reinikainen, K., Kaukoranta, E., Hamalainen, M., Ilmoniemi, R., Penttinen, A., Salminen, J., Teszner, D., 1984. Somatosensory evoked cerebral magnetic fields from SI and SII in man. Electroencephalogr. Clin. Neurophysiol. 57, 254–263.

Hari, R., Karhu, J., Hamalainen, M., Knuutila, J., Salonen, O., Sams, M., Vilkman, V., 1993. Functional organization of the human first and second somatosensory cortices: a neuromagnetic study. Eur. J. Neurosci. 5, 724–734.

Harrison, R.V., Harel, N., Panesar, J., Mount, R.J., 2002. Blood capillary distribution correlates with hemodynamic-based functional imaging in cerebral cortex. Cereb. Cortex 12, 225–233.

Hashimoto, I., Mashiko, T., Imada, T., 1996. High-frequency magnetic

signals in the human somatosensory cortex. Electroencephalogr. Clin. Neurophysiol., Suppl. 47, 67–80.

Haueisen, J., Schack, B., Meier, T., Curio, G., Okada, Y., 2001. Multiplicity in the high-frequency signals during the short-latency somatosensory evoked cortical activity in humans. Clin. Neurophysiol. 112, 1316–1325.

Helmholtz, H., 1853. Ueber einige gesetze der vertheilung elektrischer strome in korperlichen leitern, mit anwendung auf die thierischelektrischen versuche. Ann. Phys. Chem. 89, 211–233, 353–377.

Hirata, M., Kato, A., Taniguchi, M., Ninomiya, H., Cheyne, D., Robinson, S.E., Maruno, M., Kumura, E., Ishii, R., Hirabuki, N., Nakamura, H., Yoshimine, T., 2002. Frequency-dependent spatial distribution of human somatosensory evoked neuromagnetic fields. Neurosci. Lett. 318, 73–76.

Inoue, T., Shimizu, H., Nakasato, N., Kumabe, T., Yoshimoto, T., 1999. Accuracy and limitation of functional magnetic resonance imaging for identification of the central sulcus: comparison with magnetoencephalography in patients with brain tumors. NeuroImage 10, 738–748.

Jack Jr., C.R., Thompson, R.M., Butts, R.K., Sharbrough, F.W., Kelly, P.J., Hanson, D.P., Riederer, S.J., Ehman, R.L., Hangiandreou, N.J., Cascino, G.D., 1994. Sensory motor cortex: correlation of presurgical mapping with functional MR imaging and invasive cortical mapping. Radiology 190, 85–92.

Kakigi, R., Hoshiyama, M., Shimojo, M., Naka, D., Yamasaki, H., Watanabe, S., Xiang, J., Maeda, K., Lam, K., Itomi, K., Nakamura, A., 2000. The somatosensory evoked magnetic fields. Prog. Neurobiol. 61, 495–523.

Kober, H., Nimsky, C., Moller, M., Hastreiter, P., Fahlbusch, R., Ganslandt, O., 2001. Correlation of sensorimotor activation with functional magnetic resonance imaging and magnetoencephalography in presurgical functional imaging: a spatial analysis. NeuroImage 14, 1214–1228.

Korvenoja, A., Wikstrom, H., Huttunen, J., Virtanan, J., Laine, P., Aronen, H.J., Seppalainen, A.M., Ilmoniemi, R.J., 1995. Activation of ipsilateral primary sensorimotor cortex by median nerve stimulation. NeuroReport 6, 2589–2593.

Korvenoja, A., Huttunen, J., Salli, E., Pohjonen, H., Martinkauppi, S., Palva, J.M., Lauronen, L., Virtanen, J., Ilmoniemi, R.J., Aronen, H.J., 1999. Activation of multiple cortical areas in response to somatosensory stimulation: combined magnetoencephalographic and functional magnetic resonance imaging. Hum. Brain Mapp. 8, 13–27.

Krings, T., Buchbinder, B.R., Butler, W.E., Chiappa, K.H., Jiang, H.J., Cosgrove, G.R., Rosen, B.R., 1997. Functional magnetic resonance imaging and transcranial magnetic stimulation: complementary approaches in the evaluation of cortical motor function. Neurology 48, 1406–1416.

Kurth, R., Villringer, K., Mackert, B.M., Schwiemann, J., Braun, J., Curio, G., Villringer, A., Wolf, K.J., 1998. fMRI assessment of somatotopy in human Brodmann area 3b by electrical finger stimulation. NeuroReport 9, 207–212.

Kurth, R., Villringer, K., Curio, G., Wolf, K.J., Krause, T., Repenthin, J., Schwiemann, J., Deuchert, M., Villringer, A., 2000. fMRI shows multiple somatotopic digit representations in human primary somatosensory cortex. NeuroReport 11, 1487–1491.

Lin, W., Kuppusamy, K., Haacke, E.M., Burton, H., 1996. Functional MRI in human somatosensory cortex activated by touching textured surfaces. J. Magn. Reson. Imag. 6, 565–572.

Logothetis, N.K., Guggenberger, H., Peled, S., Pauls, J., 1999. Functional imaging of the monkey brain. Nat. Neurosci. 2, 555–562.

Logothetis, N.K., Pauls, J., Augath, M., Trinath, T., Oeltermann, A., 2001. Neurophysiological investigation of the basis of the fMRI signal. Nature 412, 150–157.

Makela, J.P., Kirveskari, E., Seppa, M., Hamalainen, M., Forss, N., Avikainen, S., Salonen, O., Salenius, S., Kovala, T., Randell, T., Jaaskelainen, J., Hari, R., 2001. Three-dimensional integration of brain anatomy and function to facilitate intraoperative navigation around the sensorimotor strip. Hum. Brain Mapp. 12, 180–192.

Maldjian, J.A., Gottschalk, A., Patel, R.S., Detre, J.A., Alsop, D.C., 1999. The sensory somatotopic map of the human hand demonstrated at 4 Tesla. NeuroImage 10, 55–62.

Matsuura, K., Okabe, Y., 1997. A robust reconstruction of sparse biomagnetic sources. IEEE Trans. Biomed. Eng. 44, 720–726.

Menon, R.S., Luknowsky, D.C., Gati, J.S., 1998. Mental chronometry using latency resolved functional MRI. Proc. Natl. Acad. Sci. U. S. A. 95, 10902–10907.

Moore, C.I., Stern, C.E., Corkin, S., Fischl, B., Gray, A.C., Rosen, B.R., Dale, A.M., 2000. Segregation of somatosensory activation in the human rolandic cortex using fMRI. J. Neurophysiol. 84, 558–569.

Morioka, T., Mizushima, A., Yamamoto, T., Tobimatsu, S., Matsumoto, S., Hasuo, K., Fujii, K., Fukui, M., 1995. Functional mapping of the sensorimotor cortex: combined use of magnetoencephalography, functional MRI, and motor evoked potentials. Neuroradiology 37, 526–530.

Mosher, J.C., Leahy, R.M., 1998. Recursive MUSIC: a framework for EEG and MEG source localization. IEEE Trans. Biomed. Eng. 45, 1342–1354.

Mueller, W.M., Yetkin, F.Z., Hammeke, T.A., Morris III, G.L., Swanson, S.J., Reichert, K., Cox, R., Haughton, V.M., 1996. Functional magnetic resonance imaging mapping of the motor cortex in patients with cerebral tumors. Neurosurgery 39, 515–520 (discussion 520–521).

Nakamura, A., Yamada, T., Goto, A., Kato, T., Ito, K., Abe, Y., Kachi, T., Kakigi, R., 1998. Somatosensory homunculus as drawn by MEG. NeuroImage 7, 377–386.

Narici, L., Forss, N., Jousmaki, V., Peresson, M., Hari, R., 2001. Evidence for a 7- to 9-Hz ''sigma'' rhythm in the human SII cortex. NeuroImage 13, 662–668.

Ogawa, S., Lee, T.M., 1990a. Magnetic resonance imaging of blood vessels at high fields: in vivo and in vitro measurements and image simulation. Magn. Reson. Med. 16, 9–18.

Ogawa, S., Lee, T.M., Kay, A.R., Tank, D.W., 1990b. Brain magnetic resonance imaging with contrast dependent on blood oxygenation. Proc. Natl. Acad. Sci. U. S. A. 87, 9868–9872.

Ogawa, S., Lee, T.M., Nayak, A.S., Glynn, P., 1990c. Oxygenation-sensitive contrast in magnetic resonance image of rodent brain at high magnetic fields. Magn. Reson. Med. 14, 68–78.

Ogawa, S., Tank, D.W., Menon, R., Ellermann, J.M., Kim, S.G., Merkle, H., Ugurbil, K., 1992. Intrinsic signal changes accompanying sensory stimulation: functional brain mapping with magnetic resonance imaging. Proc. Natl. Acad. Sci. U. S. A. 89, 5951–5955.

Oldfield, R.C., 1971. The assessment and analysis of handedness: the Edinburgh inventory. Neuropsychologia 9, 97–113.

Pantev, C., Gallen, C., Hampson, S., Buchanan, S., Sobel, D., 1991. Reproducibility and validity of neuromagnetic source localization using a large array biomagnetometer. Am. J. EEG Technol. 31, 83–101.

Pardo, J.V., Wood, T.D., Costello, P.A., Pardo, P.J., Lee, J.T., 1997. PET study of the localization and laterality of lingual somatosensory processing in humans. Neurosci. Lett. 234, 23–26.

Phillips, J.W., Leahy, R.M., Mosher, J.C., 1997. MEG-based imaging of focal neuronal current sources. IEEE Trans. Med. Imag. 16, 338–348.

Pollok, B., Moll, M., Schmitz, F., Muller, K., Schnitzler, A., 2002. Rapid mapping of finger representations in human primary somatosensory cortex applying neuromagnetic steady-state responses. NeuroReport 13, 235–238.

Polonara, G., Fabri, M., Manzoni, T., Salvolini, U., 1999. Localization of the first and second somatosensory areas in the human cerebral cortex with functional MR imaging. AJNR Am. J. Neuroradiol. 20, 199–205.

Puce, A., Constable, R.T., Luby, M.L., McCarthy, G., Nobre, A.C., Spencer, D.D., Gore, J.C., Allison, T., 1995. Functional magnetic resonance imaging of sensory and motor cortex: comparison with electrophysiological localization. J. Neurosurg. 83, 262–270.

Roberts, T.P., Rowley, H.A., 1997. Mapping of the sensorimotor cortex: functional MR and magnetic source imaging. AJNR Am. J. Neuroradiol. 18, 871–880.

Roberts, T., Rowley, H., Kucharczyk, J., 1995a. Applications of magnetic source imaging to presurgical brain mapping. Neuroimaging Clin. N. Am. 5, 251–266.

Roberts, T.P., Zusman, E., McDermott, M., Barbaro, N., Rowley, H.A., 1995b. Correlation of functional magnetic source imaging with intraoperative cortical stimulation in neurosurgical patients. J. Image Guid. Surg. 1, 339–347.

Robinson, S.E., Vrba, J., 1998. Functional neuroimaging by Synthetic Aperture Magnetometry (SAM). Biomag.

Rosen, B.R., Buckner, R.L., Dale, A.M., 1998. Event-related functional MRI: past, present, and future. Proc. Natl. Acad. Sci. U. S. A. 95, 773–780.

Roux, F.E., Ibarrola, D., Tremoulet, M., Lazorthes, Y., Henry, P., Sol, J.C., Berry, I., 2001. Methodological and technical issues for integrating functional magnetic resonance imaging data in a neuronavigational system. Neurosurgery 49, 1145–1156 (discussion 1156–1157).

Scannell, J.W., Young, M.P., 1999. Neuronal population activity and functional imaging. Proc. R. Soc. Lond., B Biol. Sci. 266, 875–881.

Scherg, M., von Cramon, D., 1985. A new interpretation of the generators of BAEP waves I–V: results of a spatio-temporal dipole model. Electroencephalogr. Clin. Neurophysiol. 62, 290–299.

Scherg, M., Ebersole, J.S., 1993. Models of brain sources. Brain Topogr. 5, 419–423.

Scherg, M., Bast, T., Berg, P., 1999. Multiple source analysis of interictal spikes: goals, requirements, and clinical value. J. Clin. Neurophysiol. 16, 214–224.

Stefanacci, L., Reber, P., Costanza, J., Wong, E., Buxton, R., Zola, S., Squire, L., Albright, T., 1998. fMRI of monkey visual cortex. Neuron 20, 1051–1057.

Stippich, C., Freitag, P., Kassubek, J., Soros, P., Kamada, K., Kober, H., Scheffler, K., Hopfengartner, R., Bilecen, D., Radu, E.W., Vieth, J.B., 1998. Motor, somatosensory and auditory cortex localization by fMRI and MEG. NeuroReport 9, 1953–1957.

Stippich, C., Hofmann, R., Kapfer, D., Hempel, E., Heiland, S., Jansen, O., Sartor, K., 1999. Somatotopic mapping of the human primary somatosensory cortex by fully automated tactile stimulation using functional magnetic resonance imaging. Neurosci. Lett. 277, 25–28.

Suk, J., Ribary, U., Cappell, J., Yamamoto, T., Llinas, R., 1991. Anatomical localization revealed by MEG recordings of the human somatosensory system. Electroencephalogr. Clin. Neurophysiol. 78, 185–196.

Tesche, C.D., 1996. MEG imaging of neuronal population dynamics in the human thalamus. Electroencephalogr. Clin. Neurophysiol., Suppl. 47, 81–90.

Tesche, C.D., Karhu, J., 1997. Somatosensory evoked magnetic fields arising from sources in the human cerebellum. Brain Res. 744, 23–31.

Uutela, K., Hamalainen, M., Somersalo, E., 1999. Visualization of magnetoencephalographic data using minimum current estimates. NeuroImage 10, 173–180.

Van Veen, B.D., van Drongelen, W., Yuchtman, M., Suzuki, A., 1997. Localization of brain electrical activity via linearly constrained minimum variance spatial filtering. IEEE Trans. Biomed. Eng. 44, 867–880.

Vrba, J., Anderson, G., Betts, K., Burbank, M.B., Cheung, T., Cheyne, D., Fife, A.A., 1998. 151-Channel whole-cortex MEG system for seated or supine positions. Biomag.

Widrow, B., Stearns, S., 1985. Beamformers with superresolution: adaptive signal processing. Adaptive Signal Processing. Prentice-Hall, Inc., Englewood Cliffs, pp. 445–455.

Williamson, S.J., Kaufman, L., 1981. Biomagnetism. J. Magn. Magn. Mater. 22, 129–201.

Yetkin, F.Z., Mueller, W.M., Morris, G.L., McAuliffe, T.L., Ulmer, J.L., Cox, R.W., Daniels, D.L., Haughton, V.M., 1997. Functional MR activation correlated with intraoperative cortical mapping. AJNR Am. J. Neuroradiol. 18, 1311–1315.

Yousry, T., Schmid, U.D., Schmidt, D., Heiss, D., Jassoy, A., Eisner, W., Reulen, H.J., Reiser, M., 1995. The motor hand area. Noninvasive detection with functional MRI and surgical validation with cortical stimulation. Radiologe 35, 252–255.